Journal of Biomedical Materials Research Part A

WILEY

Society For Biomaterials

RESEARCH ARTICLE OPEN ACCESS

The Potential of Aloe Vera in Solution and in Blended Nanofibers Containing Poly (3-Hydroxybutyrate-Co-3-Hydroxyvalerate) as Substrates for Neurite Outgrowth

María-del-Mar Romero-Alemán[1,2] | José-Manuel Pérez-Galván[1] | José-Enrique Hernández-Rodríguez[3] | Maximina Monzón-Mayor[2]

[1]Instituto Universitario de Investigaciones Biomédicas y Sanitarias, Universidad de las Palmas de Gran Canaria, Las Palmas, Spain | [2]Departamento de Morfología, Universidad de Las Palmas de Gran Canaria, Las Palmas, Spain | [3]Departamento de Enfermería, Universidad de las Palmas de Gran Canaria, Las Palmas, Spain

Correspondence: María-del-Mar Romero-Alemán (mariadelmar.romero@ulpgc.es)

Received: 4 June 2024 | **Revised:** 22 September 2024 | **Accepted:** 14 October 2024

Funding: This study was supported by Consejería de Educación del Gobierno de Canarias (SolSubC200801000281); Universidad de Las Palmas de Gran Canaria (ULPGC2013-12); Agencia Canaria de Investigación, Innovación y sociedad de la Información (CEI2018-34); Cabildo Insular de Gran Canaria (C2016/39; C2017/100), and Mancomunidad del Sureste de Gran Canaria (C2017-13; C2018-23).

Keywords: aligned scaffolds | axon regeneration | electrospinning | organotypic DRG explants | processed aloe vera | tissue engineering

ABSTRACT

This pilot study investigated the potential of aloe vera (AV) to promote neurite outgrowth in organotypic dorsal root ganglia (DRG) explants ($n = 230$) from neonatal rats ($n = 15$). Using this in vitro model of acute axotomy, we assessed neurite outgrowth exceeding 1.5 times the explant diameter (viable explants) and measured the longest neurite length. These parameters were evaluated under control conditions and in cultures supplemented with commercial AV and four aligned scaffolds: poly-L-lactate (PLLA), polydioxanone (PDS), poly(3-hydroxybutyrate-co-3-hydroxyvalerate) (PHBV), and blended PHBV/AV. After 6 days of culture, explants were immunostained using neuron-specific marker Tuj1 and Schwann cell marker S100. Measurements were obtained with Image J software and analyzed using Jamovi 2.3. In control and AV dilution media, the study revealed radial tissue growth from the explant body with randomly oriented neurites, whereas in all scaffolds, bidirectional tissue growth occurred parallel to nanofibers. Binomial logistic regression analyses indicated that viable explants were more likely in the control group compared to PDS ($p = 0.0042$) and PHBV ($p < 0.0001$), with non-significant differences when compared to AV dilution, PLLA, and PHBV/AV. AV dilution showed a greater association with viable explants than PLLA ($p = 0.0459$), while non-significant difference was found between AV dilution and PHBV/AV. Additionally, the PHBV/AV scaffold predicted higher odds of viable explants than PLLA ($p = 0.0479$), PDS ($p = 0.0001$), and PHBV ($p < 0.0001$). Groups with similar probabilities of obtaining viable explants (control, AV dilution, and PHBV/AV) exhibited non-significant differences in their longest neurite lengths. In conclusion, control, AV dilution, and PHBV/AV yielded the highest probability of developing viable explants and the longest neurite lengths. This is the first study demonstrating the direct permissiveness of AV for axonal outgrowth. Furthermore, the blended PHBV/AV scaffold showed significant potential as a suitable scaffold for axonal regrowth and Schwann cell migration, ensuring controlled tissue formation for tissue engineering applications.

1 | Introduction

The nervous system plays a critical role in maintaining homeostasis within the body, regulating inflammation, and promoting healing throughout different organs. Traumatic injuries to peripheral nerves and to densely innervated organs, like the skin, can cause long-term dysfunction [1]. Autologous nerve/skin grafting, the gold standard treatment for extensive tissue loss, is limited by donor availability. This highlights the need of new biomaterials that integrate nervous tissue and facilitate successful reinnervation of target tissues, ultimately determining the efficacy of grafts.

Aloe barbadensis Miller, also known as AV, has gained recognition for its potential health benefits, including antimicrobial effects, immune stimulation, and promoting skin regeneration, review in [2]. The beneficial properties of AV are primarily attributed to the gel found within its leaves. The most studied bioactive components are acemanann, a beta-(1,4)-acetylated soluble polymannose, and aloin, an anthraquinone glycoside. However, industrial processing can alter the original polysaccharides' structure compromising their physiological and pharmaceutical effects [3] for tissue engineering approaches.

Several studies have documented neuroprotective effect of AV in cultured neurons [4, 5], hippocampus, and cerebral cortex [6] as well as its antiepileptic effect in rats [7]. However, studies on its permissiveness for axonal outgrowth are lacking to date. The present study is additive to the field since AV in solution or combined in blended electrospun fibers has not been previously studied in the context of DRG neurite outgrowth in vitro. This is relevant because successful tissue repair relies on reinnervation, a process heavily influenced by glial cells [8–10]. The skin is a sensory organ primarily innervated by DRG neurons. Considering this background, we selected organotypic DRG explants as model to investigate the specific effects of AV on peripheral nervous tissue in an isolated setting.

Developing biocompatible and biodegradable scaffolds could control tissue formation. These scaffolds should ideally support axon growth, Schwann cell migration, and surrounding connective tissue integration. Electrospinning is a versatile method for creating membranes of ultrafine polymer fibers. By adjusting electrospinning parameters, researchers can control fiber diameter and alignment, mimicking the structure of the extracellular matrix found in tissues/organs of interest. Successful neurite outgrowth from primary sensory neuron cultures were reported on electrospun nanofibrous films of PDS [11], PLLA [12–14], PLCL poly(L-Lactide-co-caprolactone) [15], poly-acrylonitrile methylacrylate (PAN-MA) [16], poly(propylene carbonate) (PPC) [17], silk fibroin [18], and poly(methyl methacrylate) (PMMA) [19]. In all these studies, electrospun nanofibers directed neurite extension parallel to the alignment of the nanofibers. Aligned scaffolds resulted in longer neurite extension compared to random scaffolds (Table 1). Unfortunately, comparing published results was challenging due to significant variations in the experimental designs. These variations included the source of DRG neurons (organotypic explants from rodents/chickens, embryonic versus postnatal animals, commercially available neurons), culture duration, addition/omission of growth factors in the culture media, and criteria used to measure neurite length (from the midline vs. borders of the explant body). Considering this heterogeneity, the present study introduces aligned PHBV and PHBV/AV scaffolds as new materials for testing nervous tissue growth using organotypic DRG explants. Additionally, aligned PLLA and PDS scaffolds are included as positive controls to facilitate proper comparisons. Other authors reported PHBV/collagen nanofibers and PHBV microspheres as scaffolds for PC12 cells [20, 21]. Different studies on PHBV fibers revealed that can be degraded without any harmful products, they are highly biocompatible for clinical trials uses [22].

Organotypic DRG explants are multicellular in vitro models that preserve both cytoarchitecture and the interactions among neurons, Schwann cells, and connective cells that form the tissue, providing a close approximation to in vivo models. Thus, DRG explants can be considered in vitro models of acute axotomy [23] and valuable tools for the screening of potential treatments as scaffolds for axon regrowth, guidance, and functional regeneration. Growth factors (e.g., NGF, NT-3) are necessary for the DRG neuron survival in neonatal rats [24] and increase the longitude of the longest neurite and the area occupied by neurite arborization in comparison to control conditions [25]. Organotypic culture assays in the present study were developed in growth factor-free media to isolate the effect of tested materials despite a trophic-factor dependence of DRG neurons to survive in neonatal rodents.

This retrospective and experimental study aims to investigate the potential of processed AV gel and electrospun scaffolds as biomaterials supporting peripheral nervous tissue growth. The intention is to bridge the gap in knowledge regarding commercial AV's potential for neurite outgrowth and explore the synergistic effect when combined with electrospun nanofibers. The experimental design (Figure 1) contemplates six types of culture conditions (independent variables). The study focuses on four research questions (RQs) involving the ultrastructure of scaffolds (RQ1), the growth pattern of the nervous tissue (RQ2), the rate of viable explant (RQ3), and the longest neurite length (RQ4). An overview of the research design and methods used to answer the specific RQs are detailed in Table 2.

2 | Materials And Methods

2.1 | Commercial Aloe Vera Product and Quality Control

A commercially available aloe wvera (AV) for oral use (Luciano Reverón e Hijos SL) was obtained from *Aloe barbadensis* plantations in the Canary Islands, Spain. The concentration of acemannan was 12.85% in fresh sample using ^{1}H NMR spectrometry (Brito-Casillas, personal communication).

The quantification of aloin in commercial AV sample was achieved using ultra-performance liquid chromatography–tandem mass spectrometry (UPLC-MS/MS) according to the method described in the literature [26] with minor modifications. A tube containing 40 mg of AV sample in 1 mL of extraction solution (ACN:H_2O, 40:60) was homogenized in a vortex for 30 s and in a ultrasound bath for 10 min. Afterwards, the tube was centrifuged at 4000 rpm for 12 min. Finally, the supernatants were filtered using a syringe filter of 0.22 μm before UPLC/MS–MS injection. The concentration of aloin was obtained in a Waters ACQUITY UPLC system which consisted in a chromatographic binary

TABLE 1 | Background on neurite outgrowth from dorsal root ganglia (DRG) neurons on polymer scaffolds.

Nanofiber film	Diameter (nm) Mean ± SD	Alignment	Animal and type of DRG culture	Culture media	Days of culture	Neurite length (μm)	References
PDS[a] PDS + Astroc.[b]	2000–3000	Aligned	Rat (E16) Dissociated neurons	EMEM 5% FBS 0,01% NGF	10	1600[a] 2800[b]	[11]
PLLA	524 ± 305	High aligned[c] Med. aligned[d] Low-aligned[e]	Rat (E15) DRG explants	Neurobasal 5% FCS	3	760 ± 71[c] 656 ± 52[d] 631 ± 32[e]	[12]
PLLA	1325 ± 383[f] 759 ± 179[g] 293 ± 65[h]	Aligned	Chick (E9) DRG explants	Neurobasal NGF 50 ng/mL	5	1450[f] 1400[g] 1000[h]	[13]
PLLA[i] PLLA-LN-ads[j] PLLA-LN1[k] PLLA-LN5[l]	320 ± 42[i] 384 ± 78[j,k,l]	Non-aligned	Rat (E15) DRG explants	Neurobasal NT3 (30 ng/mL)	7	600[I] 700[j] 1200[k] 1600[l]	[14]
PLCL[m] PLCL-CNT[n]	1300–1500	Aligned	Rat Commercial DRG neurons	PN Basal Media PN growth media	6	273 ± 20[m] 376 ± 37[n]	[15]
PAN-MA	800 ± 96	Aligned	Rat (P1) DRG explants	DMEM/F12 10% FBS NGF (50 ng/mL)	7	1212 ± 131	[16]
PPC	800–1200	Aligned[o] Non-aligned[p]	Rat (P1) DRG explants	DMEM/F12 10% FBS NGF (60 ng/mL)	7	2537 ± 987[o] 493 ± 50[p]	[17]
SF[q] SF-NGF[r] SF-CNTF[s] SF-NGF-CNTF[t]	854 ± 87	Aligned	Rat (1–3 months) Dissociated neurons	F12 medium	3	60 ± 28[q] 192 ± 80[r] 78 ± 39[s] 124 ± 45[t]	[18]
PMMA	490 ± 04	Aligned[u] Non-aligned[v]	Rat (P2) Dissociated neurons	F12 medium	3	321 ± 79[u] 230 ± 54[v]	[19]

Note: Superscript in each row identify related data.

Abbreviations: CNT, carbon nanotube; CNTF, Ciliary NeuroTrophic Factor; DMEM, Dulbecco's modified Eagle's medium; EMEM, Eagle's Minimum Essential Medium; LN, Laminin; NGF, nerve growth factor; NT3, neurotrophin-3; PAN-MA, poly-acrylonitrile methylacrylate; PDS, polydioxanone; PL, polylysine; PLCL, Poly(L-Lactide-cocaprolactone); PLLA, poly-L-lactate; PMMA, Poly(methyl-methacrylate); PNGM, peripheral neuron growth medium; PPC, Poly(propylene carbonate); SF, Silk fibroin.

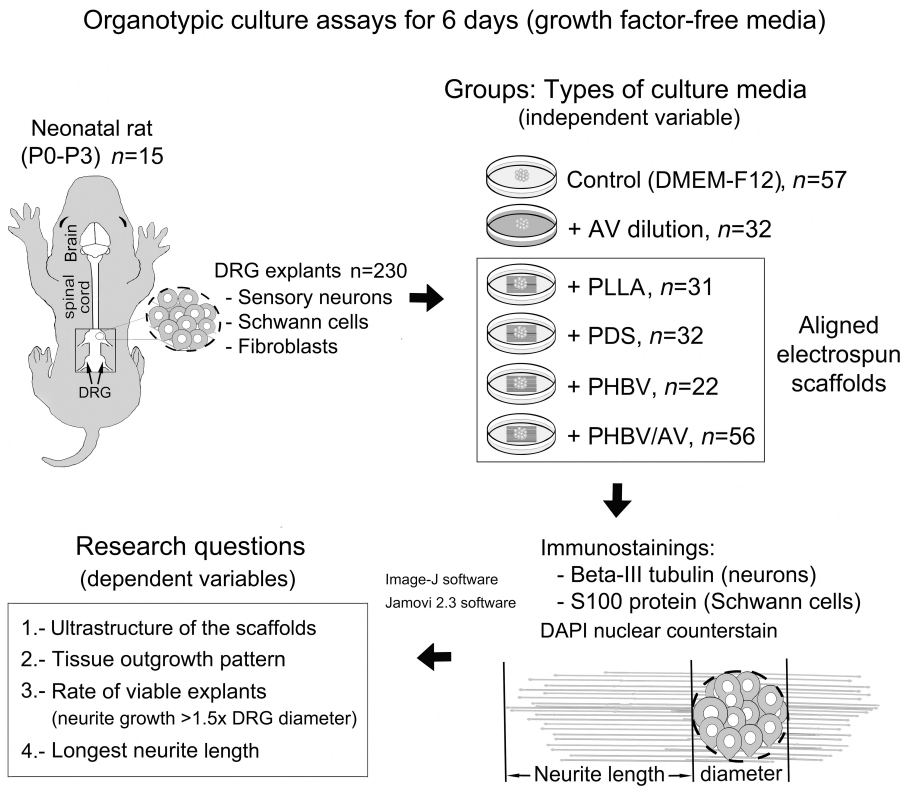

FIGURE 1 | Summary of the study design. Organotypic culture assays were performed using DRG explants from neonatal rats. Neurite extension and Schwann cell migration were compared after 6 days of culture under both control and experimental conditions. AV, aloe vera; DMEM/F12, Dulbecco's Modified Eagle's Medium; DRG, Dorsal Root Ganglion; PHBV, Poly (3-hydroxybutyrate-co-3-hydroxyvalerate); PDS, Polydioxanone; PLLA, Poly-L-lactate.

pump, a 2777 sample manager, a column manager, and a triple quadrupole detector with an electrospray interface (ESI), all from Waters (Milford, MA, USA). Briefly, the primary stock solution was prepared by dissolving an appropriate amount of aloin standard (Sigma-Aldrich) in methanol to obtain a concentration of 100 mg/L. The working solutions were prepared daily by dilution of stock solution to the required concentrations. The chromatographic analysis was performed in an ACQUITY BEH C_{18} analytical column (50 × 2.1 mm, 1.7 μm) from Waters (Milford, MA, USA) and the mobile phase was water (A) and methanol (B) both with 0.5% of acetic acid. The detection of aloin was performed using the electrospray ionization technique in negative mode (ESI–). The specific transition was 417.4—> 297.2 m/z for aloin quantification and 417.4—> 268.8 m/z for aloin confirmation. The aloin ion fragment 297.2 m/z corresponded to the loss of $[C_4H_8O_4]^-$, whereas that of 268.8 m/z corresponded to the loss of $[C_5H_9O_5]^-$.

2.2 | Nanofiber Fabrication by Electrospinning

The procedure for nanofiber fabrication was patented [27]. Briefly, three pure polymer solutions of 10 wt% PHBV, 8 wt% PLLA, and 15 wt% PDS (all from Sigma-Aldrich; Prod. n° 403,121, P1566 and 719,846, respectively) were dissolved for 24 h in Hexafluoro-2-propanol (HFIP, Sigma-Aldrich). The AV juice was lyophilized using a freeze dryer (Christ Gamma 1–15 LSC) and then dissolved in HFIP for 24 h to the concentration of 50 mg/mL. After filtration 10 wt% PHBV were added to obtain the blended polymer solution of PHBV/AV.

Four different aligned nanofibers were obtained by electrospinning of these polymer solutions: PLLA, PDS, PHBV, and PHBV/AV. Each solution was delivered by a syringe pump (Harvard Apparatus PhD Ultra) with a needle (G20, 0.9 mm diameter) and a tip, to which an electrode is attached. A flow rate was used at a humidity of 62% and at a room temperature of 25°C. A voltage of was applied by a high-voltage power supply (Spellman 60 N300). The target wheel (90 mm diameter/12 mm wide) was rotated to produce aligned fiber bundles. The specific electrospinning parameters (voltage, tip to collector distance, flow rate, collector rotation speed) for each solution are shown in Table 8.

2.3 | Nanofiber Characterization: Morphology, Diameter, Alignment, and Porosity

Three batches of each nanofiber scaffold (PHBV, PDS, PLLA, and PHBV/AV) were coated with gold using a sputter coater (BAL-TEC SCD 005) and examined using a scanning electron microscope (SEM, JSM 6300, JEOL, Japan) with an accelerating voltage of 15 kV.

The morphology of each nanofiber scaffolds was described using representative SEM micrographs. These images were also analyzed using image J software (https://imagej.nih.gov/ij/, RRID:SCR_003070) to measure the fiber diameter ($n = 100$), alignment ($n = 4$) and porosity ($n = 4$) of scaffolds. Samples were randomly selected from 3 different batches.

TABLE 2 | Research questions, designs and methods.

Specific research questions		Research design and methods
RQ1	Are there ultrastructural differences among scaffolds?	Morphologycal descriptions of scaffolds using SEM images. Analysis of SEM images using the image J software for quantification of fiber diameter ($n = 100$/group), coherency (alignment) ($n = 4$/group), and porosity ($n = 4$/group). Statistical analysis using the ANOVA test for data that met criteria for normality and homoscedasticity (fiber coherency and porosity) or the Kruskal-Wallis test for data that did not meet these criteria (fiber diameter).
RQ2	Does the type of culture medium affect the growth pattern of the nervous tissue?	Morphologycal descriptions of DRG explants after 6 days of culture using specific immunostainings to detect neurons (Tuj1), Schwann cells (S100), and nuclear counterstain (DAPI).
RQ3	RQ3.1 Do the experimental media modify the probability of obtaining viable explants compared to the control group? RQ3.2 Are viable explants more likely in presence of certain scaffolds? RQ3.3 Are viable explants more likely in presence of scaffolds or AV?	A viable explant is defined by neurite outgrowth exceeding 1.5 times the explant diameter. After counting viable and non-viable explants in both control and experimental groups, we used the Chi-squared test and various binomial logistic regression models to assess the probability of obtaining viable explants (yes/no). This assessment involved all groups ($n = 230$, Model 1) to answer RQ3.1, only scaffolds ($n = 141$, Model 2) to answer RQ3.2, and all groups ($n = 230$, Model 3) to answer RQ3.3
	RQ3.4 Do the fiber diameter, alignment and scaffold porosity influence the explant viability?	The significant differences in these variables among scaffolds would allow the transformation of continuous data into ordinal scales. Chi-squared test to evaluate the likelihood of obtaining viable explants (yes/no, $n = 141$) among different variable ranges.
RQ4	Do groups with the highest rate of viable explant exhibit differences in their longest neurite length?	The distance measurements were obtained from the borders of each DRG explant to the furthest extent of overall neurite outgrowth. Kruskal-Wallis tests and post hoc pairwise comparisons ($n = 120$).

Abbreviations: AV, aloe vera; RQ, research question; SEM, Scanning electron microscopy.

Fiber alignment was quantified as a coherency value using the Orientation J plug-in for the dominant direction in Image J [28] as described by other authors [29]. Coherency is a measure of the degree to which structures are oriented with a value of 0 (or 0%) for a completely isotropic image and a value of 1 (or 100%) for highly oriented structures.

The porosity of scaffolds was calculated per square micron area following a previously described procedure [30]. The free area in SEM images was divided by the total sample area using the equation below. The average diameter was used for the fiber area.

$$\text{Porosity} = (\text{Total sample area} - \text{Total fiber area}/\text{Total sample area})^{*} 100.$$

2.4 | Animals and DRG Extraction

The DRG ($n = 230$) were isolated from 15 Sprague Dawley rats (P0-P3) in accordance with the European and Spanish ethical guidelines (2010/63/UE and R.D. 53/2013, respectively) and approved by the Comité Ético de Bienestar Animal (CEBA) of the Universidad de Las Palmas de Gran Canaria (ULPGC) (ref. 004/2013 CEBA-ULPGC).

2.5 | DRG Neurite Outgrowth Assays

The in vitro procedure for the control assay was described previously by our group [31]. Briefly, for substrate preparation, plastic coverslips were incubated (1 h, 37°C) with 50 μg/mL poly-L-lysine (Sigma-Aldrich, Seelze, Germany) in ddH_2O. After thorough rinsing in ddH_2O, coverslips were incubated (1 h, 37°C) with 20 μg/mL laminin (Sigma-Aldrich) in PBS. Rat DRG were dissected in Dulbecco's modified Eagle's medium (DMEM/F12) (1:1) (Sigma-Aldrich), free of connective tissue and nerve roots, and cut into 200 μm thick slices using a McIlwain tissue chopper. The fragments were resuspended in the mentioned medium and passed repeatedly through a Pasteur pipette with a rounded tip to dissociate the tissue mechanically. Then, the culture medium was supplemented with 10% fetal calf serum, 0.4% methyl cellulose, 100 μM putrescine, 20 nM progesterone, 15 nM triiodothyronine, 1% insulin-transferin-sodium selenite and antimicrobial solution (1:100; all from Sigma-Aldrich) and plated on coverslips coated with poly-L-lysine/laminin which were rinsed in medium and immediately used for cell and tissue culture. Similar studies included growth factors (NGF, NT-3) in the culture media (Table 1), this was omitted in our assays. The DRG neurons were cultured in a humidified incubator for 6 days at 37°C in the presence of 5% CO_2. The culture medium was renewed after 3 days by removing it with suction.

Experimental neurite outgrowth assays were performed in presence of commercial AV for oral administration diluted at 1:50 and 1:75 (v:v) in the culture media, according to previous experiments of our group using raw AV [32], and on four aligned nanofiber membranes (PLLA, PDS, PHBV, and PHBV/AV) which were fabricated as described below. Pieces of around 5 × 5 mm

of each membrane were sterilized by irradiation with a commercial ultraviolet (UV) germicide lamp ($\lambda = 254$ nm) at 25 cm for 35 min [33]. Then, these membrane pieces were placed on coverslips and coated with poly-L-lysine/laminin as described above. Afterwards, DRG extracts were plated on membranes and rinsed in the supplemented DMEM/F12 (1:1) medium for immediate incubation in the same conditions mentioned above.

2.6 | Immunostainings and Image Acquisition

At the seventh day of incubation, the coverslip cultures containing DRG explants were fixed in 4% paraformaldehyde (Sigma-Aldrich) in 0.1 M phosphate-buffered saline (PBS; Sigma-Aldrich) for 30 min at 4°C. After washing in PBS, they were blocked in PBS containing 1% bovine serum albumin (BSA; Sigma-Aldrich) for 1 h and subsequently incubated (overnight at 4°C–8°C) with primary antibodies for single and double immunofluorescence. Single immunostaining was performed using mouse mAB to neuron-specific beta-III tubulin (Tuj-1; R&D Systems cat# MAB1195, RRID:AB_357520; 1:500 dilution) while double-immunolabeling occurred for the simultaneous detection of beta-III tubulin and the Schwann cell-specific S100 protein using the pAB rabbit anti-cow S100 (Dako; cat# Z0311; 1/250 dilution).

After washing in PBS, cultures were incubated with secondary antibody anti-mouse Cy3 (Jackson Immunoresearch cat# 715–165-151; RRID:AB_2315777; 1:1000 dilution) and anti-rabbit Alexa Fluo 488 (Molecular Probes; 1/500 dilution) for 1 h at room temperature. Cell nuclei were counterstained with 4′, 6-diamidino-2-phenylindole dihydrochloride (DAPI; 0.5 μg/mL in PBS; Sigma-Aldrich) for 10 min. Finally, coverslip cultures were mounted in Mowiol (Hoechst, Frankfurt, Germany) and stored in the dark at 4°C–8°C until examination. Negative controls were treated identically, except for replacing the monoclonal antibody with the corresponding isotype control antibody, or, except for omission of either the primary or both the primary and secondary antibodies. No staining above endogenous background levels was detectable in these controls.

Acquisition of immunofluorescence images was carried out on a Zeiss Axiovert 200 M microscope equipped with Plan-Neofluar objectives. Images were acquired with an Axiocam high-resolution monochromatic CCD camera, controlled by Zeiss Axiovision software (V4.6; RRID:SCR_002677). Images were acquired under identical exposure times and conditions for controls and experimental groups. Exposure times were generally shorter than 10 s and no detectable photobleaching occurred during image acquisition. Images of each experiment were imported into Adobe Photoshop CS4 (RRID:SCR_002078) for images editing and assembly. In those cases, in which contrast and brightness values were adjusted, images from control and experimental cultures were treated identically.

2.7 | Evaluation of Neurite Outgrowth: Viable DRG Explants and Longest Neurite Length

Neurite outgrowth was initially evaluated by determining the number of viable and nonviable DRG explants per group. Viable DRG explants displayed neurite outgrowth longer than 1.5 times the diameter of the DRG body [13]. At least three independent experiments with tissues from three different animals were performed for each group. For all experiments, images of the four quadrant projections were obtained using the 10X objective. The quantification of the neuron-specific immunostaining required the composition of a complete image of each sample by unifying the images of the four quadrant projections in a same picture. Then, the complete images were imported into the Image J software (https://imagej.nih.gov/ij/, RRID:SCR_003070).

A random sample of viable explants ($n = 10$) displaying similar diameter was selected for further analysis of the longest neurite outgrowth. The distance measurements were obtained from the borders of each DRG explant to the furthest extent of overall neuritic outgrowth [11]. The longest neurites (2–4 per explant) corresponding to control and experimental explants were measured for statistical analyses.

2.8 | Statistical Analyses

Raw data were collected in Excel files and transferred to the statistic program Jamovi 2.3.24 [34]. The level of statistical significance was set at $p < 0.05$. The p-value was coupled with effect size and 95% IC metrics whenever possible to determine the strength of the differences, supporting the biomedical relevance of findings. n: sample size. The dependent variables on nanofiber coherency ($n = 4$) and porosity ($n = 4$) were analyzed using Anova and post hoc Tukey tests, as the data met the criteria for normality and homoscedasticity. Accordingly, these data were presented as mean ± standard deviation (SD). In contrast, analyses of nanofiber diameter ($n = 100$) and the longest neurite length in a random sample of viable explants ($n = 120$) were conducted using the non-parametric Kruskal-Wallis test and post hoc Dass-Steel-Critchlow-Fligner (DSCF) comparisons, with these data presented as median ± interquartile range (IQR). The nominal dependent variable defined by the rate of viable explants (yes/no) was analyzed using the chi-squared test of association for independent samples. Binomial logistic regression was also performed to assess the likelihood of obtaining viable explants (yes) among different groups ($n = 230$) and among the four scaffolds ($n = 141$). We assessed the continuous dependent variable represented by the longest neurite length using a random sample of viable explants ($n = 40$) that did not differ significantly in the diameter of their DRG bodies.

3 | Results

3.1 | Commercial AV Product and Bioactive Components

The most studied bioactive components of AV are acemannan, a beta-(1,4)-acetylated soluble polymannose, and aloin, an anthraquinone glycoside. Specifically, 1H NMR spectrometry revealed that fresh AV drink samples contained 12.85% (w/v) of acemannan (Brito-Casillas, personal communication) and 2.24 ± 0.17 ppm of aloin, as detected by the UPLC-MS/MS

method, which was well below the international limits for oral consumption (< 10 ppm) to avoid laxative effects.

3.2 | RQ1: Are There Ultrastructural Differences Among Scaffolds?

The SEM images showed the predominance of aligned nanofibers in all scaffolds: PLLA (Figure 2A), PDS (Figure 2B), PHBV (Figure 2C), and PHBV/AV (Figure 2D). Interestingly, PHBV/AV fibers exhibited rougher surfaces (insert in Figure 2D) compared to the smoother surfaces observed in other fibers (inserts in Figure 2A–C). These scaffolds were characterized according to the nanofiber diameter, alignment (coherency), and porosity per square micron area (Table 3, Figure 2E–G).

3.2.1 | Nanofiber Diameter

Nanofiber diameter showed significant differences among groups according to the non-parametric Kruskal-Walli's test ($p < 0.0001$, $\varepsilon^2 = 0.56$). The post hoc DSCF pairwise comparisons showed significant differences between groups ($p < 0.0001$), except between PHBV and PHBV/AV ($p = 0.8167$). Consequently, PLLA fibers were the thinnest with median (IQR) values of 362 nm (295–428.25 nm) whereas PDS fibers, with values of

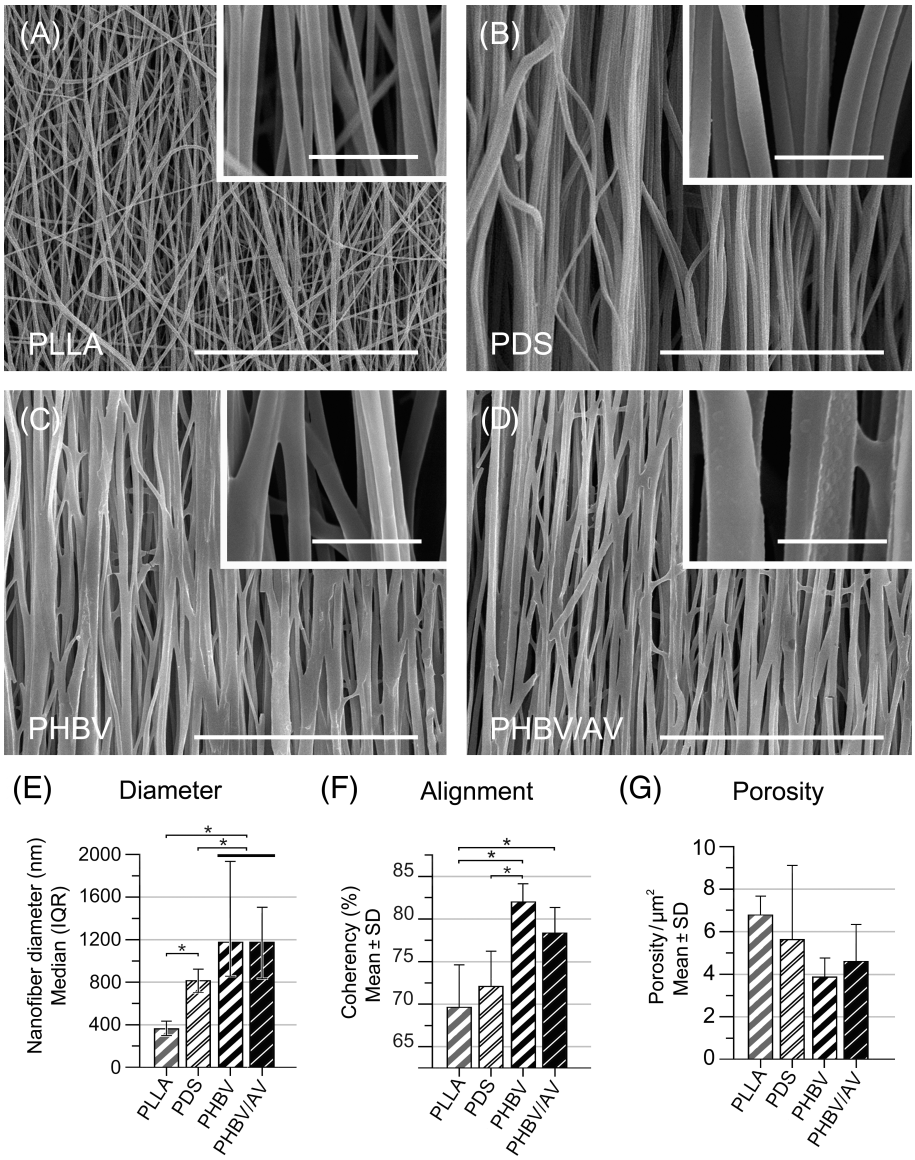

FIGURE 2 | Scanning electron microscopy images. These images show the fiber surfaces in electrospun scaffolds made from poly-L-lactate (PLLA in A), polydioxanone (PDS in B), poly (3-hydroxybutyrate-co-3-hydroxyvalerate (PHBV in C), and a blend of PHBV and aloe vera (PHBV/AV in D). Crossing fibers are observed in the PLLA scaffold (A) but are scarcely detected in the PDS (B), PHBV (C), and PHBV/AV scaffolds (D). PHBV/AV fibers exhibit irregular surfaces (inset in D), in contrast to the smooth surfaces observed in PLLA (inset in A), PDS (inset in B), and PHBV fibers (inset in C). Differences in nanofiber diameter (E), coherency (alignment) (F), and porosity per square micron area (G) are graphically represented. Data meeting the assumptions of normality and homoscedasticity are expressed as mean ± standard deviation (for coherency and porosity). Otherwise, median and interquartile range are reported (for diameter). Asterisks (*) indicate significant differences between groups. Bars: 60 µm. Insets: 6 µm.

TABLE 3 | Nanofiber characterization: Diameter, alignment (coherency), and porosity.

	Diameter (nm)		Alignment Coherency (%)	Porosity/μm²
Scaffold sample	**Mean ± SD**	**Median (IQR)**	**Mean ± SD**	**Mean ± SD**
PLLA	389.11 ± 139.01	[1] 362 (295; 428.25)[a]	69 ± 5[a]	6.92 ± 0.83
PDS	890.85 ± 328.23	[2] 802 (723; 937)[b]	72 ± 4[a,c]	5.75 ± 3.52
PHBV	1490.14 ± 873.39	[3] 1181 (835; 1969)[c]	81 ± 2[b]	3.97 ± 0.98
PHBV/AV	1287.16 ± 577.08	[3] 1181 (821.25; 1502)[c]	78 ± 2[b,c]	4.63 ± 1.75

Note: Diameter ($n = 100$/sample); Alignment and Porosity ($n = 4$/sample). Different superscripts in the same column (a, b, c) indicate significant differences. Accordingly, the sequence of numbers between brackets [1–3] represent the convertion of data into an ordinal scale with [1] denoting the lowest value.
Abbreviations: AV, aloe vera; PLLA, poly-L-lactate; PDS, polydioxanone; PHBV, poly(3-hydroxybutyrate-co-3-hydroxyvalerate).

TABLE 4 | The probability of viable explants (yes) per group is expressed as ratio, percentage and 95% CI.

		p (viable explants = yes)		
Group	***n***	**Ratio**	**%**	**95% CI**
Control	57	47/57	82.46	70–90
AV dilution	32	31/32	96.87	81–100
PLLA	31	24/31	77.42	60–89
PDS	32	17/32	53.12	36–69
PHBV	22	3/22	13.64	4–35
PHBV/AV	56	52/56	92.86	82–97
Total	230	174/230	75.65	

Abbreviations: AV, aloe vera; *p*, probability; PLLA, poly-L-lactate; PDS, polydioxanone; PHBV, poly (3-hydroxybutyrate-co-3-hydroxyvalerate).

802 nm (723–937 nm), were significantly thicker. However, PHBV and PHBV/AV were the thickest with 1181 nm (835–1969 nm) and 1181 nm (821.25–1502 nm) respectively. Despite the lack of significant differences, PHBV scaffolds showed higher variability in fiber diameter compared to PHBV/AV (Table 3). The significant differences in fiber diameter allowed the transformation of continuous data into an ordinal scale (Table 3) to evaluate the probability of obtaining viable explants (Table 4) among scaffolds (see below).

3.2.2 | Nanofiber Coherency (Alignment)

Fiber alignment in the scaffolds was quantified as coherency values ranging from 0% for completely random orientation to 100% for highly oriented fibers (Table 3, Figure 2F). PLLA showed the lowest coherency values (69 ± 5) followed by PDS (72 ± 4). Accordingly, SEM images apparently revealed more crossing fibers in PLLA scaffolds (Figure 2A) than others (Figure 2B–D). The higher coherency values were detected in PHBV (81 ± 2) and PHBV/AV (78 ± 2). ANOVA and post hoc Tukey analyses revealed significant differences in coherency between PHBV-PDS ($p = 0.0146$, Cohen's $d = 2.60$), PHBV-PLLA ($p = 0.0013$, Cohen's $d = 3.62$) and PHBV/AV-PLLA ($p = 0.0150$, Cohen's $d = 2.59$). However, non-significant differences were also observed between PHBV-PHBV/AV, PHBV/AV-PDS, and PLLA-PDS (Table 3) which did not allow to obtain a clear ordinal scale to evaluate the probability of obtaining viable explants.

3.2.3 | Nanofiber Porosity

The quantification of porosity per square micron area in the different scaffolds (Table 3) showed non-significant differences according to the ANOVA test ($p = 0.2483$). The lack of significant differences in scaffold porosity prevented measuring the impact of this variable.

In summary, there are relevant ultrastructural differences among scaffold involving (1) morphology: smooth surfaces in PLLA, PDS, PHBV, and rough surface in PHBV/AV, (2) fiber diameter: the thinnest (PLLA), intermediate (PDS), the thickest (PHBV and PHBV/AV), (3) Coherency (alignment): the lowest (PLLA) to the highest aligned (PHBV and PHBV/AV). In contrast, the scaffolds showed non-significant differences in porosity.

3.3 | RQ2: Does the Type of Culture Medium Affect the Growth Pattern of the Nervous Tissue?

Tuj1-positive neurons in the explant body exhibited a radial outgrowth pattern with randomly organized neurites distally in control media (Figure 2A,A') and in media supplemented with AV drink at 1/50 (Figure 2B,B') and 1/75 (Figure 2C,C'). Additionally, DAPI staining revealed sensory neuron nuclei in the explant body, along with migrating S100-positive Schwann cells (not shown) and putative S100-negative fibroblasts (not shown), which supported the growing neurites. Differences in the rate of viable explants among control ($n = 57$), AV diluted 1/50 ($n = 15$), and AV diluted 1/75 ($n = 17$) were statistically non-significant according to binomial logistic regression analysis (not shown). For simplicity, a single AV group (AV dilution, $n = 32$) was considered in the present study (Figure 2D).

In contrast, DRG explants displayed a predominant bidirectional tissue growth that mimicked the alignment of electrospun fibers in PLLA (Figure 3A,A'), PDS (Figure 3B,B'), PHBV (not shown), and blended PHBV/AV scaffolds (Figure 3C,C'). DAPI-positive nuclei along growing neurites were identified as S100-positive Schwann cells and putative S100-negative fibroblasts (Figure 3C', bottom-right insert) supporting neurite outgrowth.

In summary, the type of culture media influenced the tissue growth pattern. A radial pattern emanating from the explant body was observed in both the control and AV dilution culture media, while a bidirectional pattern was noted in the presence

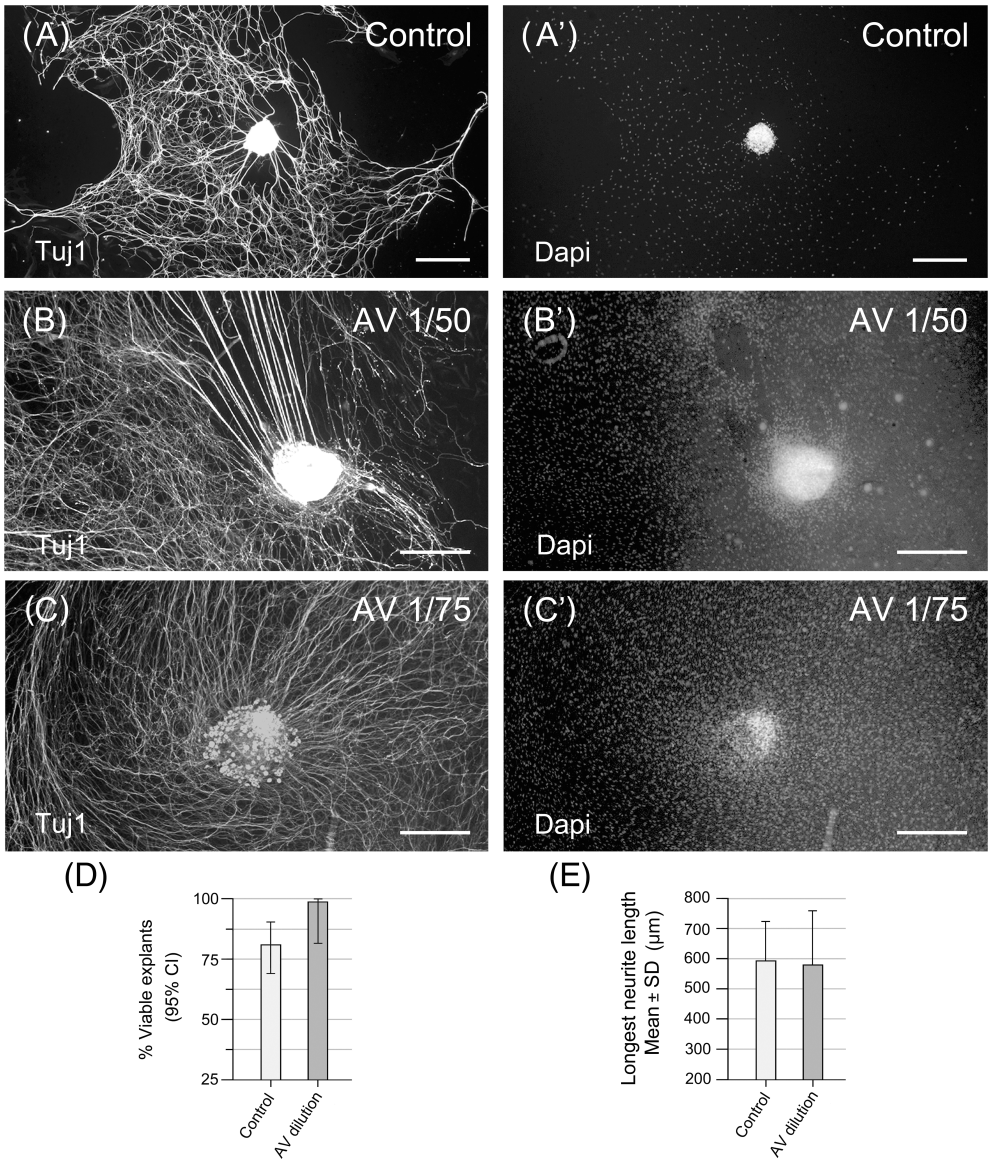

FIGURE 3 | Representative immunofluorescent images of DRG explants in control media (A-A') and experimental media supplemented with aloe vera (AV) drink at dilutions of 1/50 (B-B′) and 1/75 (C-C′). Tuj1-positive neurons in the explant body (A, B, C) exhibited a radial outgrowth pattern with randomly organized neurites. The DAPI-positive nuclei (A′, B′, C′) outside the explant bodies correspond to putative Schwann cells and fibroblasts accompanying the growing neurites. Data on the probability of obtaining neurite outgrowth exceeding 1.5 times the diameter of the explants (viable explants) (D) and the longest neurite length (E) are graphically represented. Non-significant differences were observed. Data from the AV dilutions (1/50 and 1/75) were combined into a single group ($n = 32$). Control group ($n = 57$). Bars: 200 µm.

of the four scaffolds, corresponding to their alignment. The primary components of the growing tissue were Tuj1-positive neurites, S100-positive Schwann cells, and putative S100-negative/DAPI-positive fibroblasts.

3.4 | RQ3: Rate of Viable Explants

3.4.1 | Do the Experimental Media Modify the Probability of Obtaining Viable Explants Compared to the Control Group?

Viable explants were defined as those exhibiting neurite outgrowth exceeding 1.5 times the diameter of their DRG bodies [13]. A total of 174 explants (75.65%) from 230 were viable (Table 4) and showed the following distribution: PHBV/AV (29.89%), Control (27.01%), AV dilution (17.82%), PLLA (13.79%), PDS (9.77%), PHBV (1.72%). High ratios of viable explants (Table 5, Figure 3D, Figure 4D) were observed in controls (82,46%) and experimental media supplemented with AV dilution (96.87%), PHBV/AV (92.86%), and PLLA (77.42%).

The association between the rate of viable explant and the type of culture medium was statistically significant with an acceptable effect size ($p < 0.0001$, Cramer's $V = 0.56$) according to the chi-squared test. The binomial logistic regression analysis (Table 5, Model 1) identified groups with a higher probability of obtaining viable explants (Control, AV dilution, PLLA, and PHBV/AV). These groups showed non-significant differences among them, except for PHBV/AV ($p = 0.0479$) and AV dilution ($p = 0.0459$),

TABLE 5 | Comparative analysis on the probability of viable explants (yes) using three logistic regression models.

Model	Predictor	*Z* (Wald test)	*p*	Odds ratio (95 CI)
1	AV dilution—Control	1.76	0.0790	6.60 (0.80; 54.13)
1	PLLA—Control	−0.57	0.5684	0.73 (0.25; 2.16)
1	PDS—Control	−2.86	0.0042[a]	0.24 (0.09; 0.64)
1	PHBV/AV—Control	1.63	0.1035	2.77 (0.81; 9.41)
1	PHBV—Control	−4.76	< 0.0001[a]	0.03 (0.01; 0.14)
1	PLLA—AV dilution	−2.00	0.0459[a]	0.11 (0.01; 0.96)
1	PHBV/AV—AV dilution	−0.76	0.4462	0.42 (0.04; 3.92)
2	PLLA—PHBV/AV	−1.98	0.0479[a]	0.26 (0.07; 0.99)
2	PDS—PHBV/AV	−3.88	0.0001[a]	0.09 (0.03; 0.30)
2	PHBV—PHBV/AV	−5.45	< 0.0001[a]	0.01 (0.00; 0.06)
2	PHBV—PDS	−2.76	0.0059[a]	0.14 (0.03; 0.57)
2	PLLA—PDS	1.99	0.0468[a]	3.03 (1.02; 9.01)
3	Scaffolds (Yes/No)	−3.64	0.0003[a]	0.24 (0.11; 0.52)
3	AV (Yes/No)	4.75	< 0.0001[a]	10.86 (4.06; 29.05)

[a]Significant differences in odds of viable explants between groups.
Abbreviations: AV, aloe vera; PLLA, poly-L-lactate; PDS, polydioxanone; PHBV, poly (3-hydroxybutyrate-co-3-hydroxyvalerate).

which had better odds compared to PLLA. However, these results should be interpreted with caution as they were close to non-significant. In contrast, PDS and PHBV showed significant lower odds in comparison to controls (Table 5, rhombs in Figure 4D) and to the other experimental groups. The logistic regression model on mentioned data was statistically significant ($p < 0.0001$, $n = 230$) and explained 39% (Nagelkerke R2) of the variance related to the presence of viable explants among groups (Table 6, Model 1).

3.4.2 | Are Viable Explants More Likely in Presence of Certain Scaffolds?

Viable explants occurred in scaffolds ($n = 141$) according to the following sequence: PHBV/AV (54.17%), PLLA (25%), PDS (17.71%), and PHBV (3.12%). Notably, PLLA, PDS, and PHBV exhibited lower odds of viable explants compared to PHBV/AV (Table 5, Model 2). The logistic regression Model 2 was statistically significant ($p < 0.0001$, $n = 141$) and explained 44% (Nagelkerke R2) of the variance related to the presence of viable explants among scaffolds (Table 6, model 2).

3.4.3 | Are Viable Explants More Likely in Presence of Scaffolds or AV?

In the logistic regression model considering the presence of both, scaffolds (PLLA, PDS, PHBV, PHBV/AV) and AV (AV dilution and PHBV/AV), in the culture media (Table 5, Model 3), the likelihood of viable explants was low in presence of scaffolds ($p = 0.0003$; OR = 0.24) but high in presence of AV ($p < 0.0001$; OR = 10.86). This model was statistically significant ($p < 0.0001$, $n = 230$) and explained 27% (Nagelkerke R2) of the variance related to the presence of viable explants among groups (Table 6, Model 3).

3.4.4 | Do the Fiber Diameter, Alignment, and Scaffold Porosity Influence the Explant Viability?

The association between nanofibers thickness ranging from the thinnest to the thickest (Table 3, superscripts a, b, c) and explant viability in scaffolds was not significant ($p = 0.0930$, Cramer's $V = 0.18$; Kendall's Tau-B $p = 0.9490$). In addition, Data on alignment and porosity were inadequate to establish ordinal scales for evaluating the impact of these variables.

In summary, AV dilution, PLLA, and, PHBV/AV did not significantly differ from the controls in terms of obtaining viable explants. However, PDS and PHBV exhibited significantly lower odds. PHBV/AV had a higher likelihood of producing viable explants than the other scaffolds. The likelihood of viable explants was higher in media containing AV (AV dilution + PHBV/AV) and lower in media containing scaffolds (PLLA + PDS + PHBV + PHBV/AV). Non-significant association was found between fiber diameter and explant viability, and the assessment of fiber alignment and scaffold porosity was not feasible.

3.5 | RQ4: Do Groups With the Highest Viable Explant Rates Exhibit Differences in Longest Neurite Length?

Viable explants were more likely in control, AV dilution, PLLA, and PHBV/AV groups, with non-significant differences in the longest neurite length among these conditions ($p = 0.2170$, $\varepsilon^2 = 0.04$, $n = 120$) (Table 7, Figure 4D,E). The longest neurite length was measured in a random sample of viable explants that exhibited non-significant differences ($p = 0.8201$, $\eta^2 = 0.02$, $n = 40$) in their DRG body diameters (Table 7).

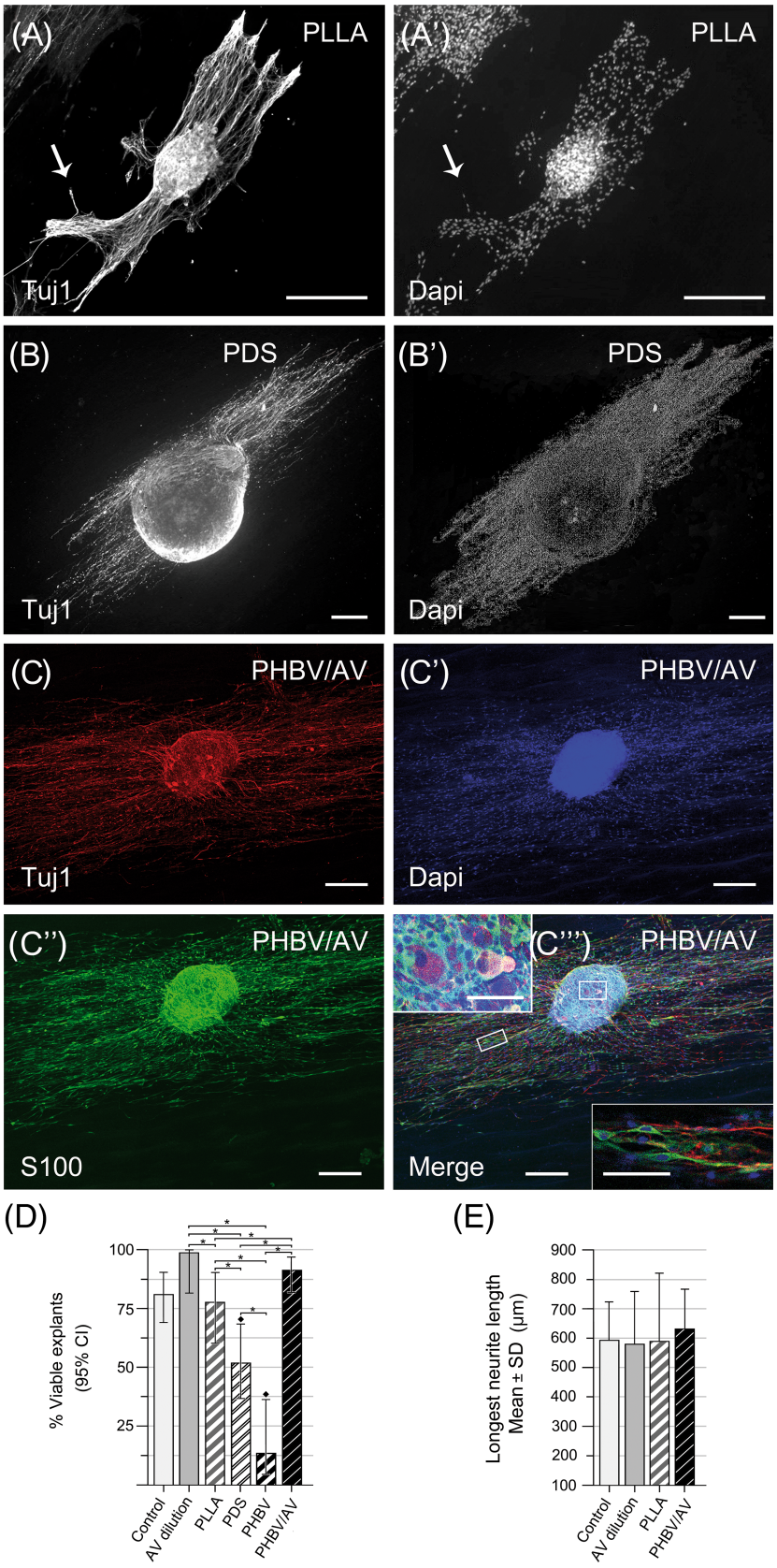

FIGURE 4 | Legend on next page

4 | Discussion

4.1 | RQ1: The Scaffolds Showed Significant Differences in Morphology, Fiber Diameter, and Alignment, but Not in Porosity

Pure fibers (PLLA, PDS, and PHBV) had smooth surfaces, unlike the rough surfaces of blended PHBV/AV. The electrospinning parameters for PHBV and PHBV/AV were similar (Table 8). Moreover, these scaffolds showed non-significant differences in median fiber diameter (Table 3, Figure 2E). The presence of AV in the polymer solution likely influenced variables affecting fiber morphology and diameter (e.g., electrostatic forces, conductivity, viscosity). Despite this, AV did not significantly alter the fiber diameter of PHBV/AV compared to pure PHBV. In contrast, other studies have reported that AV can lead to an increase or decrease in fiber diameter, as observed in PVA/AV and PCL/AV combinations, respectively [35, 36]. We hypothesize that a specific interaction between PHBV and AV maintained the fiber diameter while creating uneven surfaces (see insert in Figure 2D). PHBV scaffolds showed higher variability in fiber diameter compared to PHBV/AV (Table 3), suggesting that the presence of AV (50 mg/mL) could provide a more homogeneous fiber diameter.

Interestingly, pure PHBV displayed lower odds of viable explants compared to PHBV/AV. This suggests a potential influence of AV on factors like hydrophilicity and cell adhesion within the PHBV/AV matrix. Similar observations have been reported in culture assays using PLCL and PLCL-CNT [15] and in vivo studies on peripheral nerve regeneration with materials like PLLA, PLLA-soy protein [37], PCL, and PCL-lignin [38]. Moreover, the irregular surface and lower diameter variability of blended PHBV/AV fibers may impact the likelihood of obtaining viable explants and require further study.

According to the literature (Table 1), the longest neurite lengths from DRG neurons were observed in PLLA [13] (Wang et al., 2010), PDS [11], PAN-MA [16], and PPC [17] scaffolds which shared common features, such as fiber diameters ranging from 800 to 3000 μm and high alignment. It is noteworthy that, as observed in the present study, the average diameter of nanofibers in all these scaffolds falls outside the strict size-based definition of the nanoscale range (up to 100 nm or even 1000 nm). However, the concept of "nanofibers" can also be applied based on their biological effects, even if their dimensions deviate from the nanoscale definition [39].

In the present study, fiber characterization ranging from the thinnest and lowest aligned (PLLA: 362 μm diameter; 69% coherency), intermediate (PDS: 803 μm diameter; 72% coherency) to the thickest and highest aligned (PHBV and PHBV/

TABLE 7 | Quantitative analysis of longest neurite length in groups with higher explant viability.

	Diameter of viable explants	Longest neurite length
Sample	**Mean ± SD (*n*)**	**Mean ± SD (*n*)**
Control	210.51 ± 71.45 (10)	595.57 ± 133.17 (40)
AV dilution	215.20 ± 58.57 (10)	576.90 ± 189.86 (40)
PLLA	227.77 ± 111.04 (10)	583.39 ± 236.44 (20)
PHBV/AV	247.36 ± 120.27 (10)	633.32 ± 138.19 (20)

Note: Data are expressed as mean and standard deviation (SD) in μm.
Abbreviations: AV, aloe vera; *n*, number of experiments; PLLA, poly-L-lactate; PHBV, poly(3-hydroxybutyrate-co-3-hydroxyvalerate).

TABLE 6 | Models of binomial logistic regression.

Model	*n*	Deviance	AIC	BIC	R2N	χ^2	df	*p*
1	230	185.54	197.54	218.17	0.39	69.78	5	< 0.0001
2	141	123.70	131.70	143.49	0.44	52.90	3	< 0.0001
3	230	208.62	214.62	224.93	0.27	46.71	2	< 0.0001

Note: Model 2 is better than Model 1 and 3 according to its smaller AIC, BIC and higher R2N values.
Abbreviations: AIC: Akaike information criterion; BIC: Bayesian information criterion; *n*: number of experiments; R2N: Nagelkerke R2.

FIGURE 4 | Representative immunofluorescent images of DRG explants in culture media containing aligned scaffolds made from poly-L-lactate (PLLA in A-A′), polydioxanone (PDS in B-B′), and a blend of poly (3-hydroxybutyrate-co-3-hydroxyvalerate (PHBV) and aloe vera (AV) (PHBV/AV in C-C′-C″-C‴). The neuronal marker Tuj1 (A, B, C) and DAPI nuclear counterstaining (A′, B′, C′) revealed a predominant bidirectional tissue growth pattern. Note the neurite growth cones (arrow in A) and putative DAPI-positive Schwann cells and fibroblasts along the neurites. C-C′-C″-C‴: Double immunostaining of DRG explants for Tuj1 (C, in red) and S100 (C′, in green), along with DAPI nuclear counterstaining (C″, in blue) and merged image (C‴), in PHBV/AV scaffolds. Tuj1-positive neurites (C) and S100-positive Schwann cells (C′) were organized in parallel. C‴: The areas delimited by rectangles, inside and outside the explant body, are detailed in the top-left and bottom-right insets, respectively. The inset in the top-left corner shows Tuj1-positive neuronal perikarya and processes surrounded by abundant S100-positive Schwann cells. The yellowish staining corresponds to the neuronal bodies surrounded by satellite glial cells. The inset in the bottom-right corner shows aligned neurite outgrowth surrounded by S100-positive Schwann cells and putative S100-negative/DAPI-positive fibroblasts. (D): Significant differences (*) in the probability of obtaining viable explants between groups and in comparison to the control group (♦) are noted. (E): Groups with high probability of obtaining viable explants (Control, AV dilution, PLLA, and PHBV/AV) showed non-significant differences in the lengths of their longest neurites. Bars: 200 μm (A–C‴); 50 μm (insets in C‴).

TABLE 8 | Parameters for nanofiber fabrication by electrospinning.

Polymer solution	Concentration (%)	Voltage (Kv)	Tip to collector distance (cm)	Solution flow rate (ml/h)	Collector rotation speed (rpm)	Needle size
PLLA	8	11	11	1.2	3500	20G
PDS	15	15	11	1.9	3500	20G
PHBV	10	12	13	0.8	3000	20G
PHBV/AV[a]	10.5	12	12	0.8	3000	20G

[a]The maximum AV concentration compatible with satisfactory electrospinning was 50 mg/mL.

AV: 1181 μm diameter; 78%–81% coherency) affected the likelihood of obtaining viable explants in a complex way. For instance, PLLA and PHBV/AV showed significant differences in diameter, alignment and in the probability of obtaining viable explants (Figure 3D, Table 5). Intriguingly, PHBV and PHBV/AV showed non-significant differences in diameter and alignment but significant differences in the probability of obtaining viable explants. Polymer composition seemed as relevant and nanofiber characterization for obtaining viable explants and the longest neurite length. The impact of scaffold porosity on obtaining viable explants remained uncertain due to the lack of significant differences in porosity among the four scaffolds (Table 3) which showed significant differences in their biological effects (Table 4).

4.2 | RQ2: Radial Versus Bidirectional Tissue Growth Pattern Depending on the Type of Culture Medium

Radial tissue growth pattern from the explant body was observed in control media (Figure 2A,A') and in media supplemented with AV (Figure 2B,B',C,C'). The AV has not been previously studied in the context of neurite outgrowth. The commercially available AV drink used in this study was chosen based on its better promising outcomes for neurite outgrowth than other three commercial AV products [40], and similar results in comparison to raw AV gel [32]. This AV drink contained 12.85% acemannan in fresh sample which surpassed the average of 15 recently reported AV beverages [41]. However, industrial processing can reduce the degree of acetylation of acemannan compromising their physiological and pharmaceutical effects [3, 41]. This aspect was not evaluated in our study. The culture media containing AV dilution had 0.26% (2.6 μg/mL) acemannan and 0.045 ppm of aloin, whereas those at a 1/75 dilution involved 0.17% (1.7 μg/mL) acemannan and 0.03 ppm of aloin. These data are important for the interpretation of results since the biological effects of acemannan also depends on the dose provided to the culture media. The literature has revealed a wide range of optimal acemannan concentration depending on the biological effect under investigation. Thus, culture assays involving in human and mouse fibroblasts revealed that a 2000 μg/mL, with acetylation degree of 1.202, was optimal for inducing cell proliferation, while 5 μg/mL induced the highest cell migration after 3 h [42]. Accordingly, low acemannan concentrations of 1.7–2.5 μg/mL in the present study could exert biological effects involved in the tissue growth. It seemed too low concentrations to increase the probability of obtaining viable explants in comparison to controls (Figure 3D,E) and PHBV/AV (Figure 4D). In contrast it was enough to increase this likelihood in comparison to PLLA, PDS, and PHBV (Figure 4D). Similar results were obtained in preliminary assays of our group using raw AV gel directly from plant leaves [28]. This suggests that industrial processing of AV maintained the permissiveness for neurite outgrowth, potentially supporting its application in biomedical settings, as evidenced in rodent excisional wound healing [43].

Bidirectional tissue growth pattern occurred in the aligned scaffold in the present study as previously reported on PDS [11], PLLA [12–14], PLCL [15], PAN-MA [16], PPC [17], silk fibroin [18], and PMMA [19]. We propose that aligned scaffolds function as permissive physical barriers guiding axon outgrowth, resembling the structure of linear Büngner's bands in regenerating tissues in vivo. Supporting this notion, PLLA fibers alone can sometimes guide DRG neurites without the essential support of glial cells [13]. The range of diameters and occasional presence of crossing fibers within a single matrix could mimic the heterogeneous cellular profiles observed within Büngner's bands [8].

4.3 | RQ3-4: Rate of Viable Explants and Longest Neurite Length: Biomedical Significance and Future Considerations

Although none of the experimental media surpassed the control in terms of the probability of obtaining viable explants and the longest neurite length, our data contribute to the field in the following ways:

1. AV Dilution: The AV dilution demonstrated a significant probability of developing the mentioned biological effects, despite the low concentration of acemannan in the culture media. The holistic role of the multiple bioactive components of AV should be considered in these outcomes. This perspective opens the possibility of further optimization given the dose-dependent (and acetylation-dependent) effects of acemannan [42].
2. PHBV/AV Scaffolds: From a biomedical perspective, PHBV/AV scaffolds (and potentially PLLA, pending further investigation) offer a clear advantage over the control and AV dilution in directing nervous tissue growth, which is critical for tissue engineering applications. Furthermore, we hypothesize that the release of AV during PHBV/AV degradation could sustain long-term nervous tissue growth. This hypothesis is supported by our statistical data, which revealed that the presence of AV enhances explant viability

in the culture media. Degradation studies would be necessary to confirm this view in the future.

3. Synergistic Effects: Our statistical data revealed a significant probability of viable explants in culture media containing AV (AV dilution + PHBV/AV) (Table 5, Model 3), suggesting the possibility of synergistic effects from combining these media. This opens new directions for future research in the field.

Notably, our study achieved successful tissue growth even though the culture media lacked neurotrophins and contained potential inhibitors of neurite outgrowth, such as fetal calf serum [44]. We hypothesize that endogenous Schwann cells might be secreting nerve growth factor, and endogenous fibroblasts might be exhibiting pro-regenerative behavior, both of which could contribute to DRG neuron survival and neurite outgrowth as occurs in vivo [45]. Avoiding this exogenous supplementation in our study design was more realistic for evaluating the neurite outgrowth than those reported in similar studies, which included supplementation of growth factors with no apparent standardized criteria (see Table 1). This situation made difficult a realistic comparison of results among similar studies by different authors. From our point of view, standardized study designs in this field are still pending.

4.4 | Limitations of the Study

The main limitation of the study was the heterogeneous sample size among different groups which, along with the use of non-parametric statistics, could affect the statistical power of the findings.

5 | Conclusion

The novel findings of the current study consisted in reveling the permissiveness of commercial AV and blended electrospun PHBV/AV scaffolds for peripheral nervous tissue growth using an in vitro model of acute axotomy. Despite nonstatistical significance in comparison to controls, aligned PHBV/AV scaffolds directed the neurite outgrowth and Schwann cell migration which is of utmost importance for tissue engineering applications.

Acknowledgments

The present study was supported by Consejería de Educación del Gobierno de Canarias (SolSubC200801000281); Universidad de Las Palmas de Gran Canaria (ULPGC2013-12); Agencia Canaria de Investigación, Innovación y sociedad de la Información (CEI2018-34); Cabildo Insular de Gran Canaria (C2016/39; C2017/100), and Mancomunidad del Sureste de Gran Canaria (C2017-13; C2018-23). The authors extend their gratitude to the following collaborators: Juan F. Arbelo and Sara Diepa for their excellent technical assistance; Dr. Pedro Saavedra (Department of Mathematics, ULPGC) for his support with statistical analyses; Dr. Zoraida Sosa-Ferrera (Department of Chemistry, ULPGC), Dr. Raico Guedes-Alonso (IUNAT-ULPGC), and Dr. Ignacio Brouard (IPNA-CSIC) for their help with UPLC-MS/MS and 1H NMR analyses; and Javier González-Fernández (ITC-ULL) for his assistance with the electrospinning procedure. The collaboration of SIMACE (ULPGC) and the Electron Microscopy Service (ULL) is also appreciated.

Conflicts of Interest

The authors are co-inventors of a European patent titled "Hybrid Aloe vera Nanofibers" (PCT/ES2017/000029), owned by the Universidad de Las Palmas de Gran Canaria. This patent has not been licensed or sold to any industry. The authors confirm that this situation has not influenced the interpretation of the data presented in this paper. They have no other competing interests to declare.

Data Availability Statement

The data that support the findings of this study are available from the corresponding author upon reasonable request.

References

1. B. Laverdet, A. Danigo, D. Girard, L. Magy, C. Demiot, and A. Desmoulière, "Skin Innervation: Important Roles During Normal and Pathological Cutaneous Repair," *Histology and Histopathology* 30, no. 8 (2015): 875–892, https://doi.org/10.14670/HH-11-610.

2. M. Chelu, A. M. Musuc, M. Popa, and M. J. Calderon, "*Aloe vera*-Based Hydrogels for Wound Healing: Properties and Therapeutic Effects," *Gels* 9, no. 7 (2023): 539, https://doi.org/10.3390/gels9070539.

3. S. Rahman, P. Carter, and N. Bhattarai, "Aloe Vera for Tissue Engineering Applications," *Journal of Functional Biomaterials* 8, no. 1 (2017): 6, https://doi.org/10.3390/jfb8010006.

4. D. Lobine, M. R. Howes, I. Cummins, et al., "Bio-Prospecting Endemic Mascarene Aloes for Potential Neuroprotectants," *Phytotherapy Research* 31, no. 12 (2017): 1926–1934, https://doi.org/10.1002/ptr.5941.

5. Y. Wang, L. Cao, and G. Du, "Protective Effects of Aloe Vera Extract on Mitochondria of Neuronal Cells and Rat Brain," *Zhongguo Zhong Yao Za Zhi* 35, no. 3 (2010): 364–368, https://doi.org/10.4268/cjcmm20100324.

6. M. S. Parihar, M. Chaudhary, R. Shetty, and T. Hemnani, "Susceptibility of Hippocampus and Cerebral Cortex to Oxidative Damage in Streptozotocin Treated Mice: Prevention by Extracts of Withania Somnifera and Aloe Vera," *Journal of Clinical Neuroscience* 11, no. 4 (2004): 397–402, https://doi.org/10.1016/j.jocn.2003.09.008.

7. N. Rathor, T. Arora, S. Manocha, A. N. Patil, P. K. Mediratta, and K. K. Sharma, "Anticonvulsant Activity of Aloe Vera Leaf Extract in Acute and Chronic Models of Epilepsy in Mice," *Journal of Pharmacy and Pharmacology* 66, no. 3 (2014): 477–485, https://doi.org/10.1111/jphp.12181.

8. J. A. Gomez-Sánchez, K. S. Pilch, M. van der Lans, et al., "After Nerve Injury, Lineage Tracing Shows That Myelin and Remak Schwann Cells Elongate Extensively and Branch to Form Repair Schwann Cells, Which Shorten Radically on Remyelination," *Journal of Neuroscience* 37, no. 37 (2017): 9086–9099, https://doi.org/10.1523/JNEUROSCI.1453-17.2017.

9. V. Parfejevs, J. Debbache, O. Shakhova, et al., "Injury-Activated Glial Cells Promote Wound Healing of the Adult Skin in Mice," *Nature Communications* 9, no. 1 (2018): 236, https://doi.org/10.1038/s41467-017-01488-2.

10. R. Thompson and S. Sakiyama-Elbert, "Using Biomaterials to Promote Pro-Regenerative Glial Phenotypes After Nervous System Injuries," *Biomedical Materials* 13, no. 2 (2018): 024104, https://doi.org/10.1088/1748-605X/aa9e23.

11. W. N. Chow, D. G. Simpson, J. W. Bigbee, and R. J. Colello, "Evaluating Neuronal and Glial Growth on Electrospun Polarized Matrices: Bridging the Gap in Percussive Spinal Cord Injuries," *Neuron Glia Biology* 3, no. 2 (2007): 119–126, https://doi.org/10.1017/S1740925X07000580.

12. J. M. Corey, D. Y. Lin, K. B. Mycek, et al., "Aligned Electrospun Nanofibers Specify the Direction of Dorsal Root Ganglia Neurite Growth," *Journal of Biomedical Materials Research. Part A* 83, no. 3 (2007): 636–645, https://doi.org/10.1002/jbm.a.31285.

13. H. B. Wang, M. E. Mullins, J. M. Cregg, C. W. McCarthy, and R. J. Gilbert, "Varying the Diameter of Aligned Electrospun Fibers Alters Neurite Outgrowth and Schwann Cell Migration," *Acta Biomaterialia* 6, no. 8 (2010): 2970–2978, https://doi.org/10.1016/j.actbio.2010.02.020.

14. L. He, S. Tang, M. P. Prabhakaran, et al., "Surface Modification of PLLA Nano-Scaffolds With Laminin Multilayer by LbL Assembly for Enhancing Neurite Outgrowth," *Macromolecular Bioscience* 13, no. 11 (2013): 1601–1609, https://doi.org/10.1002/mabi.201300177.

15. G. Z. Jin, M. Kim, U. S. Shin, and H. W. Kim, "Neurite Outgrowth of Dorsal Root Ganglia Neurons Is Enhanced on Aligned Nanofibrous Biopolymer Scaffold With Carbon Nanotube Coating," *Neuroscience Letters* 501, no. 1 (2011): 10–14, https://doi.org/10.1016/j.neulet.2011.06.023.

16. V. J. Mukhatyar, M. Salmerón-Sánchez, S. Rudra, et al., "Role of Fibronectin in Topographical Guidance of Neurite Extension on Electrospun Fibers," *Biomaterials* 32, no. 16 (2011): 3958–3968, https://doi.org/10.1016/j.biomaterials.2011.02.015.

17. Y. Wang, Z. Zhao, B. Zhao, et al., "Biocompatibility Evaluation of Electrospun Aligned Poly (Propylene Carbonate) Nanofibrous Scaffolds With Peripheral Nerve Tissues and Cells In Vitro," *Chinese Medical Journal* 124, no. 15 (2011): 2361–2366.

18. T. M. Dinis, G. Vidal, R. R. Jose, et al., "Complementary Effects of Two Growth Factors in Multifunctionalized Silk Nanofibers for Nerve Reconstruction," *PLoS One* 9, no. 10 (2014): e109770, https://doi.org/10.1371/journal.pone.0109770.

19. H. Xia, Q. Chen, Y. Fang, et al., "Directed Neurite Growth of Rat Dorsal Root Ganglion Neurons and Increased Colocalization With Schwann Cells on Aligned Poly (Methyl Methacrylate) Electrospun Nanofibers," *Brain Research* 1565 (2014): 18–27, https://doi.org/10.1016/j.brainres.2014.04.002.

20. W. Chen and Y. W. Tong, "PHBV Microspheres as Neural Tissue Engineering Scaffold Support Neuronal Cell Growth and Axon-Dendrite Polarization," *Acta Biomaterialia* 8, no. 2 (2012): 540–548, https://doi.org/10.1016/j.actbio.2011.09.026.

21. M. P. Prabhakaran, E. Vatankhah, and S. Ramakrishna, "Electrospun Aligned PHBV/Collagen Nanofibers as Substrates for Nerve Tissue Engineering," *Biotechnology and Bioengineering* 110, no. 10 (2013): 2775–2784, https://doi.org/10.1002/bit.24937.

22. Ł. Kaniuk and U. Stachewicz, "Development and Advantages of Biodegradable PHA Polymers Based on Electrospun PHBV Fibers for Tissue Engineering and Other Biomedical Applications," *American Chemical Society Biomaterials Science & Engineering* 7, no. 12 (2021): 5339–5362, https://doi.org/10.1021/acsbiomaterials.1c00757.

23. N. Neacşu and M. Flonta, "Classification of Dorsal Root Ganglion Neurons From Newborn Rat in Organotypic Cultures," *Romanian Journal of Biophysics* 16, no. 2 (2006): 77–91, https://doi.org/10.1021/acsbiomaterials.1c00757.

24. H. K. Yip, K. M. Rich, P. A. Lampe, and E. M. Johnson, Jr., "The Effects of Nerve Growth Factor and Its Antiserum on the Postnatal Development and Survival After Injury of Sensory Neurons in Rat Dorsal Root Ganglia," *Journal of Neuroscience* 4, no. 12 (1984): 2986–2992, https://doi.org/10.1523/JNEUROSCI.04-12-02986.1984.

25. A. Torres-Espín, D. Santos, F. González-Pérez, J. del Valle, and X. Navarro, "Neurite-J: An Image-J Plug-In for Axonal Growth Analysis in Organotypic Cultures," *Journal of Neuroscience Methods* 236 (2014): 26–39, https://doi.org/10.1016/j.jneumeth.2014.08.005.

26. P. G. Wang, W. Zhou, W. G. Wamer, A. J. Krynitsky, and J. I. Rader, "Simultaneous Determination of Aloin A and Aloe Emodin in Products Containing Aloe Vera by Ultra-Performance Liquid Chromatography With Tandem Mass Spectrometry," *Analytical Methods* 4 (2012): 3612–3619, https://doi.org/10.1039/C2AY25599E.

27. M. Monzón-Mayor, M. M. Romero-Alemán, J. E. Hernández-Rodríguez, and J. M. Pérez-Galván, "University of las Palmas de Gran Canaria. Hybrid Aloe Vera Nanofibers," *European Patent EP3428117 (B1)* 30 (2022): 878.

28. D. Sage, and J. Orientation, "A Series of Image," *Journal of Plugins for Directional Image Analysis* 12 (2024). August 01, 2024, http://bigwww.epfl.ch/demo/orientation/.

29. R. E. Young, J. Graf, I. Miserocchi, et al., "Optimizing the Alignment of Thermoresponsive Poly(N-Isopropyl Acrylamide) Electrospun Nanofibers for Tissue Engineering Applications: A Factorial Design of Experiments Approach," *PLoS One* 14, no. 7 (2019): e0219254, https://doi.org/10.1371/journal.pone.0219254.

30. A. S. The, "Porosity of Nanofiber Layers," in *Biocomposites—Recent Advances*, eds. M. M. M. Elnashar and S. Karakuş (London, UK: IntechOpen, 2023), 40–53, https://doi.org/10.5772/intechopen.109104.

31. D. M. Lang, M. D. Romero-Alemán, B. Dobson, E. Santos, and M. Monzón-Mayor, "Nogo-A Does not Inhibit Retinal Axon Regeneration in the Lizard Gallotia Galloti," *Journal of Comparative Neurology* 525, no. 4 (2017): 936–954, https://doi.org/10.1002/cne.24112.

32. S. Montesdeoca-Santana, D. M. Lang, E. Doncel-Pérez, M. Monzón-Mayor, and M. M. Romero-Alemán, "Preliminary Assays of Dorsal Root Ganglia Axonal Regrowth in Aloe Vera Enriched Culture Medium," in *Presented at the FENS Forum* (Geneva CHE: Federation of European neuroscience Societies, 2008).

33. D. Yixiang, T. Yong, S. Liao, C. K. Chan, and S. Ramakrishna, "Degradation of Electrospun Nanofiber Scaffold by Short Wave Length Ultraviolet Radiation Treatment and Its Potential Applications in Tissue Engineering," *Tissue Engineering. Part A* 14, no. 8 (2008): 1321–1329, https://doi.org/10.1089/ten.tea.2007.0395.

34. "The jamovi project," 2022, https://www.jamovi.org.

35. D. Hikmawate, A. R. Rohmadanik, A. P. Putra, et al., "The Effect of Aloe Vera Extract Variation in Electrospun Polyvinyl Alcohol (PVA)-Aloe Vera-Based Nanofiber Membrane," *Journal of Physics: Conference Series* 1120 (2018): 012096, https://doi.org/10.1088/1742-6596/1120/1/012096.

36. S. Suganya, J. Venugopal, S. Agnes Mary, S. Ramakrishna, B. S. Lakshmi, and V. R. Giri Dev, "Aloe Vera Incorporated Biomimetic Nanofibrous Scaffold: A Regenerative Approach for Skin Tissue Engineering," *Iranian Polymer Journal* 23 (2014): 237–248, https://doi.org/10.1007/s13726-013-0219-2.

37. Q. Zhang, Z. Tong, F. Chen, et al., "Aligned Soy Protein Isolate-Modified Poly (L-Lactic Acid) Nanofibrous Conduits Enhanced Peripheral Nerve Regeneration," *Journal of Neural Engineering* 17, no. 3 (2020): 036003, https://doi.org/10.1088/1741-2552/ab8d81.

38. S. Amini, A. Saudi, N. Amirpour, et al., "Application of Electrospun Polycaprolactone Fibers Embedding Lignin Nanoparticle for Peripheral Nerve Regeneration: In Vitro and In Vivo Study," *International Journal of Biological Macromolecules* 159 (2020): 154–173, https://doi.org/10.1016/j.ijbiomac.2020.05.073.

39. P. Satalkar, B. S. Elger, and D. M. Shaw, "Defining Nano, Nanotechnology and Nanomedicine: Why Should It Matter?," *Science and Engineering Ethics* 22, no. 5 (2016): 1255–1276, https://doi.org/10.1007/s11948-015-9705-6.

40. M. M. Romero-Alemán, J. E. Hernández-Rodríguez, J. M. Pérez-Galván, and M. Monzón-Mayor, "Aloe Vera Gel and Hybrid Nanofibers of Aloe Vera Are Permissive Substrates for Neurite Outgrowth of Rat DRG Neurons In Vitro [SEHIT Abstract]," *Histology and Histopathology* 32, no. S1 (2017): 159.

41. F. Comas-Serra, P. Estrada, R. Minjares-Fuentes, and A. Femenia, "Evaluation of Acemannan in Different Commercial Beverages Containing Aloe Vera (*Aloe barbadensis* Miller) gel," *Gels* 9, no. 7 (2023): 552, https://doi.org/10.3390/gels9070552.

42. M. H. Chou, Y. H. Chen, M. T. Cheng, H. C. Chiang, H. W. Chen, and C. W. Wang, "Potential of Methacrylated Acemannan for Exerting

Antioxidant-, Cell Proliferation-, and Cell Migration-Inducing Activities In Vitro," *BioMed Central Complementary Medicine and Therapies* 23, no. 1 (2023): 204, https://doi.org/10.1186/s12906-023-04022-8.

43. J. E. Hernández-Rodríguez, J. L. Martín-Barrasa, J. Aragón-Sánchez, et al., "The Effect of Honey, Aloe Vera, and Hydrocolloid Dressing on the Healing Process of Murine Excisional Wounds," *International Journal of Lower Extremity Wounds*. Published ahead of print. November 15, 2023, https://doi.org/10.1177/15347346231214597.

44. G. E. Davis, S. D. Skaper, M. Manthorpe, G. Moonen, and S. Varon, "Fetal Calf Serum-Mediated Inhibition of Neurite Growth From Ciliary Ganglion Neurons In Vitro," *Journal of Neuroscience Research* 12, no. 1 (1984): 29–39, https://doi.org/10.1002/jnr.490120104.

45. S. G. van Neerven, P. Pannaye, A. Bozkurt, et al., "Schwann Cell Migration and Neurite Outgrowth Are Influenced by Media Conditioned by Epineurial Fibroblasts," *Neuroscience* 252 (2013): 144–153, https://doi.org/10.1016/j.neuroscience.2013.08.009.